J Physiol 587.12 (2009) pp 3009–3023

The Journal of Physiology

Developmental regulation of the intracellular Ca^{2+} sensitivity of vesicle fusion and Ca^{2+}–secretion coupling at the rat calyx of Held

Olexiy Kochubey, Yunyun Han and Ralf Schneggenburger

Laboratory of Synaptic Mechanisms, Brain-Mind Institute, École Polytechnique Fédérale de Lausanne (EPFL), 1015 Lausanne, Switzerland

Developmental refinement of synaptic transmission can occur via changes in several pre- and postsynaptic factors, but it has been unknown whether the intrinsic Ca^{2+} sensitivity of vesicle fusion in the nerve terminal can be regulated during development. Using the calyx of Held, a giant synapse in the auditory pathway, we studied the presynaptic mechanisms underlying the developmental regulation of Ca^{2+}–secretion coupling, comparing a time period before, and shortly after the onset of hearing in rats. We found an ∼2-fold leftward shift in the relationship between EPSC amplitude and presynaptic Ca^{2+} current charge (Q_{Ca}), indicating that brief presynaptic Ca^{2+} currents become significantly more efficient in driving release. Using a Ca^{2+} tail current protocol, we also found that the high cooperativity between EPSC amplitude and Q_{Ca} was slightly reduced with development. In contrast, in presynaptic Ca^{2+} uncaging experiments, the intrinsic Ca^{2+} cooperativity of vesicle fusion was identical, and the intrinsic Ca^{2+} sensitivity was slightly reduced with development. This indicates that the significantly enhanced release efficiency of brief Ca^{2+} currents must be caused by a tighter co-localization of Ca^{2+} channels and readily releasable vesicles, but not by changes in the intrinsic properties of Ca^{2+}-dependent release. Using the parameters of the intrinsic Ca^{2+} sensitivity measured at each developmental stage, we estimate that during a presynaptic action potential (AP), a given readily releasable vesicle experiences an about 1.3-fold higher 'local' intracellular Ca^{2+} concentration ($[Ca^{2+}]_i$) signal with development. Thus, the data indicate a tightening in the Ca^{2+} channel–vesicle co-localization during development, without a major change in the intrinsic Ca^{2+} sensitivity of vesicle fusion.

(Resubmitted 14 March 2009; accepted after revision 22 April 2009; first published online 29 April 2009)

Corresponding author R. Schneggenburger: Laboratory of Synaptic Mechanisms, École Polytechnique Fédérale de Lausanne (EPFL), Brain-Mind Institute, CH-1015 Lausanne, Switzerland. Email: ralf.schneggenburger@epfl.ch

For the correct functioning of neuronal networks, it is crucial that synaptic connections are formed with the appropriate strength and speed, properties which are set up during brain development. At the calyx of Held, a large glutamatergic relay synapse in the auditory brainstem, high speed of synaptic signalling is crucial for auditory information processing (Trussell, 1999), and high speed is enabled via the near-synchronous release of hundreds of transmitter quanta from the large nerve terminal. Calyces of Held are formed at postnatal days (P) ∼2–3 (Kandler & Friauf, 1993; Hoffpauir *et al.* 2006; Rodriguez-Contreras *et al.* 2008), but airborne hearing starts in rodents only at ∼P12 (Jewett & Romano, 1972; Geal-Dor *et al.* 1993). Interestingly, when comparing synaptic function before hearing onset (at ∼P5–P9) and shortly after hearing onset (at P12–P15 or older), it has been found that several pre- and postsynaptic developmental refinements occur which contribute to enhance fast signalling at the calyx of Held synapse. Thus, the presynaptic AP in the nerve terminal becomes shorter (Taschenberger & von Gersdorff, 2000; Yang & Wang, 2006), the kinetics of AMPA receptor-mediated EPSCs are speeded up (Taschenberger & von Gersdorff, 2000; Iwasaki & Takahashi, 2001) and the NMDA receptor-mediated component of the EPSC is strongly reduced with development (Futai *et al.* 2001; Joshi & Wang, 2002), although signalling via NMDA receptors remains functional (Steinert *et al.* 2008).

There is also evidence for a tightening in presynaptic Ca^{2+} channel–vesicle coupling at around the onset of hearing in mice (Fedchyshyn & Wang, 2005), based on the finding that synaptic transmission becomes less sensitive to exogenously added EGTA, a Ca^{2+} buffer with slow Ca^{2+} binding kinetics (Neher, 1998). In addition, the steepness in log–log plots of the EPSC amplitude *versus* presynaptic Ca^{2+} current charge (called the 'Ca^{2+} current–release

DOI: 10.1113/jphysiol.2009.172387

cooperativity' in what follows) can be used as an indicator of how many local Ca^{2+} channels contribute to the release control of a given vesicle. Varying the number of Ca^{2+} channels when many Ca^{2+} channels control the release of a given vesicle will create a graded variation of the 'local' $[Ca^{2+}]_i$ signal. In this case, the Ca^{2+} current–release cooperativity will be equally high as the intrinsic ('biochemical') cooperativity with which Ca^{2+} induces release ('domain overlap'; Borst & Sakmann, 1999). With fewer Ca^{2+} channels contributing to release control, however, the Ca^{2+} current–release cooperativity drops, until a value of 1 is reached in the limit of a 'single-channel' control mechanism (Yoshikami *et al.* 1989; Augustine *et al.* 1991; Meinrenken *et al.* 2002; Brandt *et al.* 2005; Gentile & Stanley, 2005). Indeed, it was found that the Ca^{2+} current–release cooperativity was reduced with development at the mouse calyx of Held, which probably indicates that fewer Ca^{2+} channels contribute to the release control of a given readily releasable vesicle (Fedchyshyn & Wang, 2005). However, it has been unknown whether the intrinsic Ca^{2+} cooperativity and sensitivity of vesicle fusion might change during development.

At the calyx of Held, presynaptic Ca^{2+} uncaging has shown a relatively high intracellular Ca^{2+} sensitivity of vesicle fusion, compatible with amplitudes of 'local' intracellular Ca^{2+} signals at the sites of vesicle fusion of only $\sim$10 μM $[Ca^{2+}]_i$ (Bollmann *et al.* 2000), or $\sim$25 μM $[Ca^{2+}]_i$ (Schneggenburger & Neher, 2000; Lou *et al.* 2005). However, Ca^{2+} uncaging has been limited to young rats (see references above) or mice (Sun *et al.* 2007) of about 7–10 days postnatally (P7–P10). To investigate a possible change in the intracellular Ca^{2+} sensitivity of vesicle fusion during development, we have established presynaptic Ca^{2+} uncaging experiments at a more mature stage of development in rats (P12–P15); a developmental stage that immediately follows the onset of hearing at $\sim$P12 in rats (Jewett & Romano, 1972). When comparing the presynaptic Ca^{2+}–secretion coupling between P8–P9 and P12–P15, we found a pronounced increase in the efficiency of brief Ca^{2+} currents in inducing release. On the other hand, the intracellular Ca^{2+} sensitivity of vesicle fusion as measured by Ca^{2+} uncaging was unchanged, or even slightly reduced, in agreement with a recent report in mice (Wang *et al.* 2008). Thus, the developmental enhancement of Ca^{2+}–secretion coupling must be caused by a tighter co-localization of readily releasable vesicles with voltage-gated Ca^{2+} channels.

Methods

Slice electrophysiology

Transverse brainstem slices of 180–200 μm thickness containing the medial nucleus of the trapezoid body (MNTB) were prepared as described previously (von Gersdorff *et al.* 1997), using a Leica VT 1000S slicer (Leica Microsystems, Wetzlar, Germany). For the dissection of the brainstem, a rat was killed quickly by decapitation without prior anaesthesia, in a procedure approved by the Veterinary office of the Canton of Vaud, Switzerland (authorization 1864). We studied two age groups of Wistar rats: postnatal days 8–9 (P8–P9, 'young' age group), and P12–P15 ('more mature' age group), with the day of birth referred to as P0. For the experiments shown in Fig. 2, transverse slices with a tilted angle of about 30 deg were made, in an attempt to cut the axons close to the calyces of Held thereby improving presynaptic voltage-clamp conditions (Borst & Sakmann, 1998). Slices were kept in an incubation chamber with a bicarbonate-buffered solution containing (in mM): 125 NaCl, 25 $NaHCO_3$, 2.5 KCl, 1.25 NaH_2PO_4, 25 glucose, 0.4 ascorbic acid, 3 *myo*-inositol, 2 sodium pyruvate, 2 $CaCl_2$ and 1 $MgCl_2$ (pH 7.4, when bubbled with 95% O_2–5% CO_2). The extracellular solution during the experiments had the same composition; tetraethylammonium chloride (TEA, 10 mM), tetrodotoxin (TTX, 1 μM), D-2-amino-5-phosphonopentanoic acid (D-AP5, 50 μM), γ-D-glutamylglycine (γ-DGG, 2 mM) and cyclothiazide (CTZ, 100 μM) were added for paired recordings (Figs 1 and 3). For the experiments in Fig. 2, γ-DGG was omitted. For postsynaptic recordings after afferent fibre stimulation (Fig. 6), D-AP5 (50 μM), CTZ (100 μM), bicuculine (10 μM) and strychnine (2 μM) were added to the extracellular solution. Afferent stimulation of presynaptic axons was performed with a concentric bipolar stimulation electrode (MCE-100; Rhodes Medical Instruments, Woodland Hills, CA, USA) placed medially to the MNTB. Experiments were done at room temperature (21–24°C).

Whole-cell recordings of visually identified presynaptic calyces and/or postsynaptic principal neurons of the MNTB were made with EPC-9/2 or EPC-10/2 double patch-clamp amplifiers (HEKA Elektronik, Lambrecht/Pfalz, Germany) in set-ups with upright microscopes under infrared gradient contrast illumination (Luigs and Neumann, Ratingen, Germany). The intracellular (pipette) solutions contained (in mM): 135 caesium gluconate, 20 TEA, 10 Hepes, 5 Na_2-phosphocreatine, 4 MgATP, 0.3 Na_2GTP, pH 7.2, to which either 100 μM or 5 mM EGTA was added for pre- or postsynaptic recordings, respectively. Pre- and postsynaptic series resistances were 15–25 MΩ (using up to 60% compensation) and 3–8 MΩ (compensation up to 85%), respectively. EPSC traces were off-line corrected for the remaining R_s error, and presynaptic Ca^{2+} currents were corrected for leak and capacitative currents with a *P*/5 protocol.

Ca^{2+} uncaging and Ca^{2+} imaging

Ca^{2+} uncaging experiments were similar to those described previously (Wölfel *et al.* 2007). In brief, the presynaptic intracellular solutions contained (in mM): 130 caesium gluconate, 20 TEA-Cl, 20 Hepes, 5 Na_2-phosphocreatine, 5 Na_2ATP, 0.3 Na_2GTP, 0.5 $MgCl_2$, 0.1 fura-2FF (TefLabs, Austin, TX, USA), DM-nitrophen (Calbiochem; 2 mM, with 1.75 mM $CaCl_2$ added); pH 7.2, 310 mosmol l^{-1}. In some experiments, a higher DM-nitrophen concentration (5 mM, with 4.52 mM $CaCl_2$ added) was used to produce post-flash $[Ca^{2+}]_i$ values up to 90 μM. An SP-20 flash lamp (Rapp OptoElectronic, Hamburg, Germany) produced a brief single flash of light (~450 μs half-width). Simulations showed that this light pulse should produce a step-like cellular $[Ca^{2+}]_i$ elevation with a 20–80% rise time of 240 μs. A dual-port epifluorescence condenser (TILL Photonics, Gräfelfing, Germany) in the microscope selected 60% of the flash lamp light and 40% of the monochromator light used to excite fura-2FF (at 350 and 380 nm) for the ratiometric measurement of post-flash $[Ca^{2+}]_i$. The relatively high intensity of the monochromator (Polychrome V, TILL Photonics) caused a slow $[Ca^{2+}]_i$ rise following weak flashes (see Fig. 3*A* and *B*; black $[Ca^{2+}]_i$ traces), and delayed the decay of $[Ca^{2+}]_i$ following flashes to higher $[Ca^{2+}]_i$.

Data analysis and model calculations

The presynaptic Ca^{2+} influx charge (Q_{Ca}) during Ca^{2+} currents (Fig. 1) was obtained by integrating the Ca^{2+} current traces, starting from the zero intercept point during the pulse to 0 mV, until $3 \times \tau_{fast}$ of a fit of the Ca^{2+} tail current decay with a double-exponential function. For the protocol using steps to +80 mV (Fig. 2), only the charge of the Ca^{2+} tail current was analysed up to a time value of $3 \times \tau_{fast}$.

To obtain transmitter release rates from paired recordings (Figs 3 and 4, obtained in the presence of 100 μM CTZ and 2 mM γ-DGG), the R_s-corrected EPSC traces were deconvolved, assuming a bi-exponential decay of the mEPSC (Neher & Sakaba, 2001). We used a standard mEPSC amplitude (q) of 15 pA for all cells in each age group. This reflects our finding that the mEPSC amplitudes were not significantly changed in this age range (see below; but see Taschenberger *et al.* 2005), and that the blocking effect of 2 mM γ-DGG in the presence of 100 μM CTZ is ~50% (see Wölfel *et al.* 2007; their Fig. 2). The deconvolution analysis assumes that the EPSC is composed of the sum of release-evoked mEPSCs, and a late current mediated by glutamate spill-over. During deconvolution, the late current is calculated based on previous release events and a model of glutamate diffusion (Neher & Sakaba, 2001). The parameters for the glutamate diffusion model were found by deconvolving the EPSC obtained in response to 'fitting protocol' stimuli (see e.g. Figs 6 and 12 of Neher & Sakaba, 2001), which were given at the start of each paired recording.

For deconvolving the EPSCs evoked by afferent fibre stimulation (Fig. 6), we determined the mEPSC parameters (amplitude, and τ_{fast} and τ_{slow} of the mEPSC decay) from measurements of spontaneous mEPSCs in each cell, and no correction for glutamate spillover was made, as in Schneggenburger & Neher (2000). Detection of mEPSCs was done with a routine written in IgorPro. The mean (± S.E.M.) mEPSC amplitudes for the data obtained in Fig. 6 (in the presence of 100 μM CTZ) were 42.0 ± 3.8 pA at P8–P9 ($n = 6$), and 40.3 ± 3.4 pA at P12–P15 ($n = 6$), and therefore, not significantly different between the two age groups ($P = 0.72$).

The cumulative release rate traces after Ca^{2+} uncaging (Fig. 4*A*) were derived by integration of the release rate traces obtained by deconvolution, without correction for readily releasable pool recovery. The integrated release rate traces were fitted with five functions: single-exponential, exponential plus line, double-exponential, double-exponential plus line, and triple-exponential (Wölfel *et al.* 2007). The best-fitting model was selected based on the Bayesian information criterion (BIC; Schwarz, 1978) by the lowest BIC value. The BIC value was calculated as: $BIC = N \cdot \ln[\sum (y_i - \hat{y}_i)^2/N] + M \cdot \ln(N)$, where N is the number of fitted data points (y_i), $\sum (y_i - \hat{y}_i)^2$ is the summed square of fit residuals, and M is the number of fit parameters used in the model. In most cases, the best-fit functions were double-exponential, double-exponential plus line, or triple-exponential functions. In these cases, we used the fast and slow time constants (τ_1, τ_2) as release time constants (Fig. 4*B*), and the corresponding amplitude values (A_1, A_2) as an estimate of the number of released vesicles in each kinetic component (Fig. 4*C* and *D*).

The five-site model of Ca^{2+} binding and vesicle fusion (Schneggenburger & Neher, 2000) was used to simultaneously fit the $[Ca^{2+}]_i$ dependence of peak transmitter release rates, release delays and times to peak release rate (Fig. 5) by minimizing the sum of logarithmized fit residuals for each fitted parameter. A 5th order adaptable step size Runge–Kutta method was used to solve the system of differential equations. The model was driven with a realistic $[Ca^{2+}]_i$ waveform simulated for the measured flash-lamp discharge. The values of interest (peak release rate, release delay at 5 released vesicles, time to peak release) were extracted from the simulated release rate trace at each $[Ca^{2+}]_i$. The vesicle pool sizes used for the fits were fixed to the average values of the fast release component (1109 and 1767 vesicles for the young, and the more mature age group; Fig. 4*C*).

The back-calculation of the 'local' $[Ca^{2+}]_i$ signal (Fig. 6*C*) used a two-sided Gaussian waveform

(Schneggenburger & Neher, 2000) with parameters A, peak local $[Ca^{2+}]_i$; t_0, time of peak; and σ_{rise}, σ_{decay} determining the rise and decay rates of the local $[Ca^{2+}]_i$. The parameters were varied until the predicted release rate matched the observed one, as determined by minimizing the weighted χ^2 value. Weighting was done with the fitted release rate trace taken to the power 0.25, which was found to improve the convergence of the fit around the peak of the release rate. The parameter σ_{rise} was constrained not to be smaller than the 20–80% rise time of the AP-evoked Ca^{2+} current in each age group. For the young age group, this value was 154 μs as measured experimentally (Müller *et al.* 2008). For the more mature age group, a value of 69 μs was used, which was found by the Hodgkin–Huxley simulation of the Ca^{2+} current during an AP (see Supplemental Fig. 3, available online only).

Data analysis and numerical simulations were performed using routines written in IgorPro 5.05 (Wavemetrics, Lake Oswego, OR, USA). Average values are reported as mean ± S.E.M., and statistical significance was assessed with a two-sample unpaired two-tailed Student's t test unless otherwise indicated. In the figures, a statistically significant difference between two sample groups is indicated by asterisks ($^*P < 0.05$; $^{**}P < 0.01$; $^{***}P < 0.001$).

Results

A leftward shift in the EPSC–presynaptic Ca^{2+} charge relation during development

We started by investigating how brief presynaptic Ca^{2+} currents become more efficient in triggering transmitter release during development of the calyx of Held synapse. During a presynaptic AP, a brief (< 0.5 ms half-width) Ca^{2+} current with a total charge of about 1 pC flows into the rat calyx of Held (Borst & Sakmann, 1998). Here, we used rectangular voltage-clamp pulses of varying lengths in the presynaptic nerve terminal (to either 0 mV, or to +80 mV in a 'tail' current protocol; see Figs 1 and 2, respectively), to measure the relationship between EPSC amplitude, and the presynaptic Ca^{2+} current integral (EPSC–Q_{Ca} relationship). We wanted to investigate whether the developmental increase in the release efficiency of brief Ca^{2+} currents (Taschenberger *et al.* 2002; Fedchyshyn & Wang, 2005) is also apparent as an absolute leftward-shift in the EPSC–Q_{Ca} relationship. Throughout this study, we compared two developmental age groups: synapses in P8–P9 rats, and in P12–P15 rats, which correspond to time intervals shortly before, and shortly after hearing onset, respectively (Jewett & Romano, 1972; Geal-Dor *et al.* 1993).

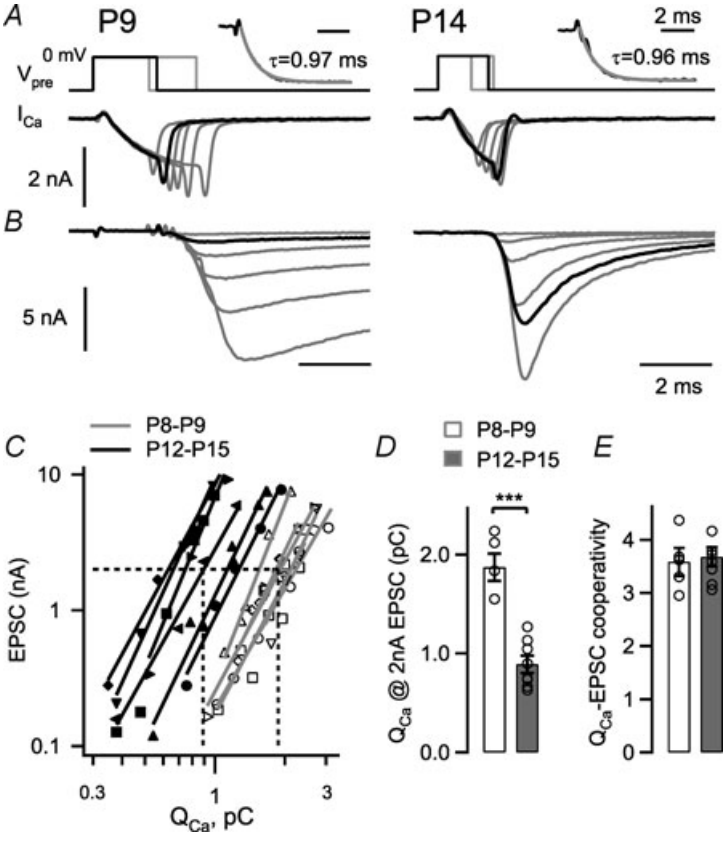

Figure 1. A pronounced leftward shift in the EPSC–presynaptic Ca^{2+} charge relation during developmental maturation
A and *B*, presynaptic Ca^{2+} currents (*A*) and the corresponding postsynaptic EPSCs (*B*) in a P9 (left) and a P14 calyx of Held synapse, with presynaptic depolarizations to 0 mV of increasing lengths. The insets in *A* show an exponential fit (grey line) to the rising phase of the Ca^{2+} currents, with time constants as indicated. The traces highlighted by black lines show presynaptic Ca^{2+} currents with similar charge transfer, which evoke an ∼9-fold larger EPSC in the P14 synapse. *C*, plot of the EPSC amplitudes as a function of the presynaptic Ca^{2+} charge, for $n = 7$ cells at P8–P9 (open symbols) and for $n = 6$ cells at P12–P15 (filled symbols). The logarithmized data set of each cell was fitted with a line, which is superimposed. Note that the data from the older age group is clearly leftward shifted. *D*, average and individual values of the presynaptic Ca^{2+} charge needed to evoke an EPSC of 2 nA. *E*, the slope values of the line fits to the EPSC amplitude *versus* Q_{Ca} data in double-logarithmic coordinates ('Ca^{2+} current–release cooperativity'). Note the unchanged value between the two age groups ($P = 0.7$).

Table 1. Parameters of presynaptic Ca^{2+} current and Ca^{2+} current density at two developmental stages

Parameter	P8–P9	P12–P15	*P* value[a]
Ca^{2+} current at 0 mV (nA)[b]	1.69 ± 0.21	1.80 ± 0.13	$P = 0.6$
	($n = 8$)	($n = 12$)	
Ca^{2+} current activation time constant (ms)[c]	1.16 ± 0.12	0.95 ± 0.05	$P = 0.11$
	($n = 8$)	($n = 13$)	
Whole-cell membrane capacitance (pF)[d]	23 ± 1.5	19.1 ± 1.3	$P = 0.035$
	($n = 9$)	($n = 14$)	
Ca^{2+} current density (pA pF^{-1})[e]	73 ± 6.1	91 ± 7.4	$P = 0.034$
	($n = 8$)	($n = 12$)	

[a]From two-sample unpaired Student's *t* test. [b]Measured as the maximal Ca^{2+} current during the step to 0 mV. [c]Measured by exponential fits to the rise of Ca^{2+} currents in response to prolonged (> 6 ms) steps to 0 mV. [d]Measured by the setting of the slow capacitance cancellation circuit of the patch-clamp amplifier. [e]Calculated by dividing the Ca^{2+} current at 0 mV by the membrane capacitance estimated in each cell.

Figure 1*A* and *B* shows experiments from a P9 rat (left panel) and from a P14 rat (right panel), representative for the two age groups studied here. Ca^{2+} currents evoked by voltage steps of increasing lengths evoked EPSCs of increasing amplitudes (Fig. 1*B*). In the cell pair from the older age group, EPSCs rose and decayed faster (Fig. 1*B*, right). As highlighted by the black traces in Fig. 1*A* and *B*, Ca^{2+} currents with similar Ca^{2+} charge transfer (~1.7 pC in this example) evoked a much larger EPSC in the P14 synapse (7.3 nA) than in the P9 synapse (0.9 nA).

When we plotted the EPSC amplitudes as a function of the presynaptic Ca^{2+} charge (Q_{Ca}) on log–log scales (Fig. 1*C*), the EPSC amplitudes measured in the more mature synapses at P12–P15 (Fig. 1*C*, filled symbols; $n = 7$ cell pairs) were consistently leftward-shifted as compared to the data obtained in younger synapses (Fig. 1*C*, open symbols; $n = 6$ cell pairs). We fitted the logarithmized data sets with lines, in order to estimate the Ca^{2+} current–release cooperativity (see Introduction), and to quantify the increased efficiency of brief Ca^{2+} current in inducing release. We found that the interpolated Ca^{2+} charge necessary to evoke an EPSC of 2 nA amplitude (Fig. 1*C*, dashed lines) was 1.97 ± 0.12 pC at P8–P9 ($n = 5$ cell pairs), and 0.89 ± 0.09 pC at P12–P15 ($n = 7$ cell pairs); and thus, significantly smaller at the more mature age ($P < 0.001$; Fig. 1*D*). The slope in the EPSC *versus* Ca^{2+} current charge (Q_{Ca}) relationship, which indicates the Ca^{2+} current–release cooperativity, was 3.58 ± 0.26 at P8–P9 ($n = 5$ cell pairs) and 3.68 ± 0.18 at P12–P15 ($n = 8$ cell pairs), and thus was not changed significantly ($P = 0.75$; see Fig. 1*E*).

We also analysed the amplitude and the activation time constant of the presynaptic whole-cell Ca^{2+} currents during prolonged (> 6 ms) steps to 0 mV, a voltage which is close to the maximal Ca^{2+} current in *I–V* curves. The resulting parameters are summarized in Table 1. The Ca^{2+} current amplitude and its activation time course were not significantly different between the two age groups (see Table 1). To estimate the Ca^{2+} current density, we normalized the Ca^{2+} current measured at 0 mV by the membrane capacitance of each calyx of Held. This revealed a slightly larger Ca^{2+} current density in more mature calyces, because the membrane capacitance was slightly smaller in the more mature calyces than in the younger ones (Table 1).

A slight decrease in the Ca^{2+} current–release cooperativity is revealed by a tail current protocol

The experiments in Fig. 1 suggest that brief Ca^{2+} currents become significantly more efficient in inducing transmitter release, mainly because of a pronounced leftward-shift in the EPSC–Q_{Ca} relation, with a largely unchanged slope. Previous experiments with a tail current protocol at the mouse calyx of Held synapse have shown, however, that the slope in the EPSC–Q_{Ca} relation was significantly reduced with development (Fedchyshyn & Wang, 2005). To resolve this apparent discrepancy, we next used a Ca^{2+} tail current protocol with brief steps to +80 mV.

Figure 2*A* and *B* shows a series of Ca^{2+} tail currents and the resulting EPSCs for an example cell pair of each age group. During the pulse to +80 mV, there was a transient outward current (Fig. 2*A*, arrow) that we interpret as gating current caused by the activation of voltage-gated channels. Following the repolarization, there was a transient inward ('tail') current flowing through the open Ca^{2+} channels. We varied the

duration of the activating pulse to +80 mV in order to recruit a varying number of Ca^{2+} channels. In some experiments, we found that it was difficult to obtain a graded Ca^{2+} tail current amplitude over a reasonably large range with steps to +80 mV, presumably because Ca^{2+} channels activate very rapidly at positive membrane potentials (Borst & Sakmann, 1998). In the experiments of Fig. 2*A* and *B*, it was possible to vary the Ca^{2+} current integral in the range of about 1 pC and below, and the slopes in the resulting EPSC–Q_{Ca} plots were 4.6 and 3.6, respectively (Fig. 2*B*, insets).

When we plotted the absolute data sets from all cells, there was again a clear leftward shift of the EPSC–Q_{Ca} relation (Fig. 2*C*). The interpolated Q_{Ca} value necessary to evoke an EPSC of 2 nA was 0.92 ± 0.06 pC at P8–P9 ($n = 8$ cell pairs), and 0.63 ± 0.07 pC at P12–P15 ($n = 5$ cell pairs; $P = 0.007$; see Fig. 2*D*). In addition to the leftward shift, the EPSC–Q_{Ca} relationship also showed a trend towards lower slopes with developmental maturation (Fig. 2*C*). Specifically, the slopes of line fits to the double-logarithmized data sets were 4.6 ± 0.2 at P8–P9 ($n = 8$ cell pairs) and 3.7 ± 0.3 at P12–P15 ($n = 5$ cell pairs; $P = 0.04$; see Fig. 2*E*); and thus, significantly lower at the more mature age. This confirms previous findings of a developmental decrease of the Ca^{2+} current–release cooperativity at the mouse calyx of Held (Fedchyshyn & Wang, 2005). Note, however, that the relative change was larger in the previous study than what we found here.

The intrinsic Ca^{2+} cooperativity of transmitter release is unchanged during synapse maturation

The experiments in Figs 1 and 2 showed a pronounced increase in the efficiency of brief presynaptic Ca^{2+} currents in evoking release, such that a 1.6- to 2-fold smaller Ca^{2+} current charge was equally efficient in inducing transmitter release in the more mature synapses. The most likely explanation for this effect is that the spatial coupling between readily releasable vesicles and Ca^{2+} channels becomes tighter with development, as has been suggested before (Fedchyshyn & Wang, 2005). It is also

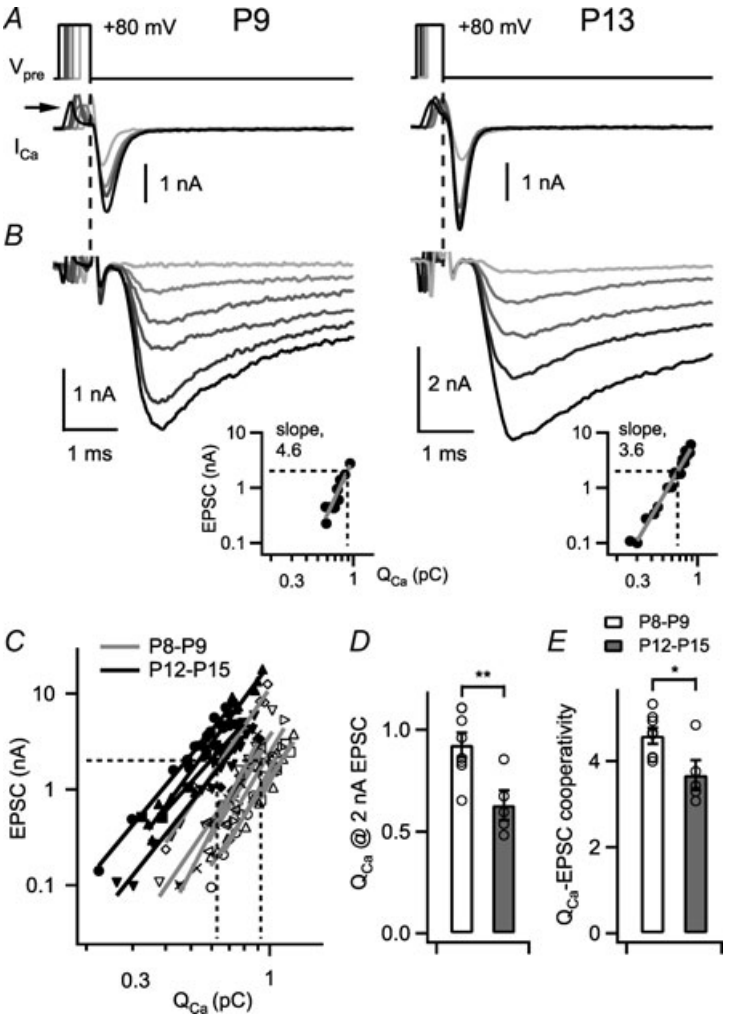

Figure 2. A slight decrease in the Ca^{2+} current–release cooperativity during developmental maturation
A and *B*, presynaptic Ca^{2+} tail currents (*A*) and the corresponding postsynaptic EPSCs (*B*) in a P9 (left) and a P13 calyx of Held synapse (right), with presynaptic depolarizations to +80 mV of varying durations. The insets in *B* show plots of the EPSC amplitude *versus* Q_{Ca} for the corresponding cells on the same scales, with slope values as indicated. *C*, plot of the EPSC amplitudes as a function of the presynaptic Ca^{2+} charge for $n = 8$ cells at P8–P9 (open symbols) and for $n = 5$ cells at P12–P15 (filled symbols). Each logarithmized data set was fitted with a line to yield the individual slope values. Note the leftward shift, and the trend towards shallower slopes in the more mature age group (P12–P15). *D*, average and individual values of the presynaptic Ca^{2+} charge needed to evoke an EPSC of 2 nA. Note the significant difference between age groups ($P = 0.007$). *E*, the slope values obtained from line fits to log–log plots of EPSC amplitude *versus* Q_{Ca}. Note the slight, but statistically significant ($P = 0.04$) reduction of the Ca^{2+} current–release cooperativity with development.

possible, however, that part of the leftward shift in the EPSC–Q_{Ca} relation (Figs 1 and 2) is caused by an increased intrinsic Ca^{2+} sensitivity of vesicle fusion. To investigate this possibility, we next performed presynaptic Ca^{2+} uncaging experiments to measure the intracellular Ca^{2+} sensitivity of vesicle fusion at two developmental stages, similar to the approach used recently by Wang *et al.* (2008) at the mouse calyx of Held. Ca^{2+} uncaging should also allow us to address the question of whether a change in the *intrinsic* Ca^{2+} cooperativity of vesicle fusion contributes to the decrease in the Ca^{2+} current–release cooperativity (Fig. 2; Fedchyshyn & Wang, 2005).

In a first series of Ca^{2+} uncaging experiments, we used a low concentration of Ca^{2+}-loaded DM-nitrophen in the presynaptic pipette solution (2 mM; see Methods). We applied several Ca^{2+} uncaging stimuli with different flash light intensities, with the aim to map out the intracellular Ca^{2+} sensitivity and Ca^{2+} cooperativity of release in a range of 2 to ~15 μM $[Ca^{2+}]_i$. At both age groups, $[Ca^{2+}]_i$ steps to low micromolar levels induced slowly rising EPSCs (Fig. 3*A* and *B*; black traces), whereas $[Ca^{2+}]_i$ steps to higher values induced more rapidly rising EPSCs with larger amplitudes (Fig. 3*A* and *B*; blue and red traces). We deconvolved the EPSCs to obtain the underlying rates of transmitter release (Fig. 3*B*, insets; Schneggenburger & Neher 2000; Neher & Sakaba, 2001). The release rates for comparable $[Ca^{2+}]_i$ steps were remarkably similar for the young and for the more mature synapse illustrated in Fig. 3*A* and *B*.

We next analysed the intrinsic Ca^{2+} cooperativity of release, by plotting the peak transmitter release rates against the post-flash $[Ca^{2+}]_i$ values, and fitting the logarithmized data sets below 10 μM $[Ca^{2+}]_i$ with a line (Fig. 3*C*; black symbols and fit lines). The analysis was restricted to below 10 μM $[Ca^{2+}]_i$ because at higher values, the relation between peak release rates and $[Ca^{2+}]_i$ starts to become more shallow (see below; Fig. 5*A*). Linear fits revealed intrinsic Ca^{2+} cooperativities of 3.5 and 3.4 for the young and for the more mature example cell pairs shown in Fig. 3. For similar experiments in a larger sample of cell

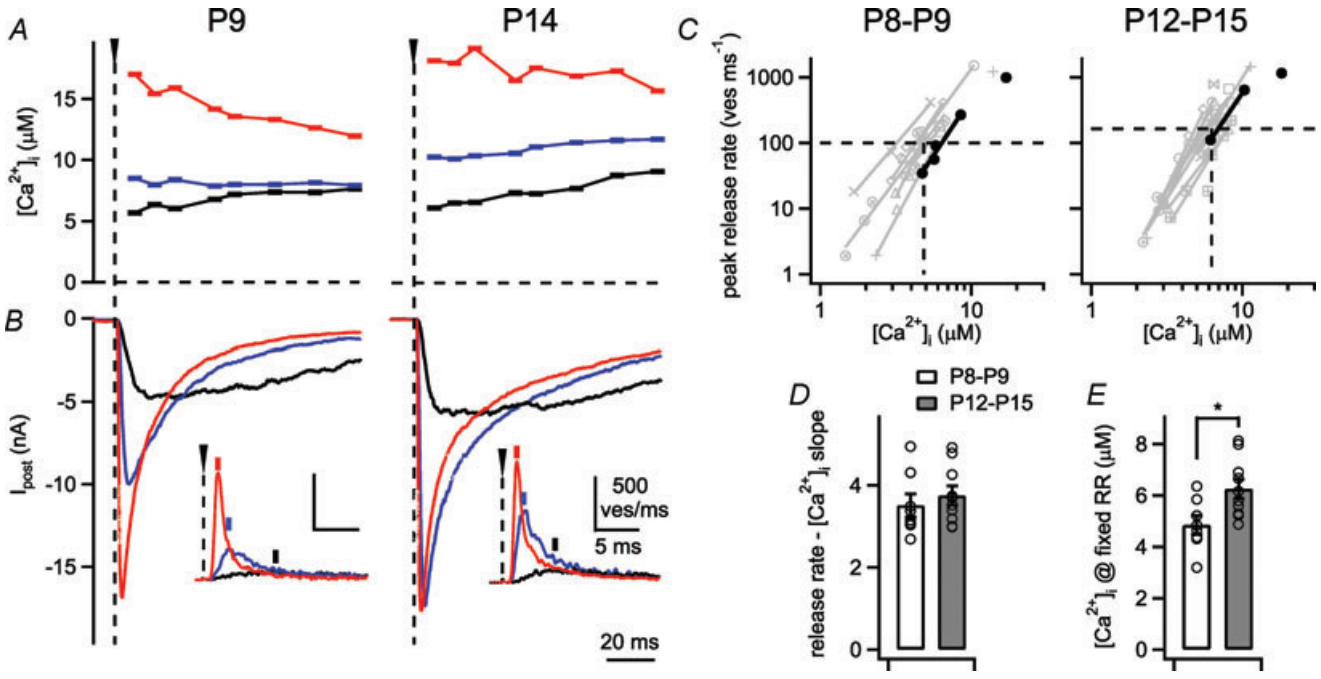

Figure 3. Ca^{2+} uncaging experiments measure the intracellular Ca^{2+} sensitivity and Ca^{2+} cooperativity of vesicle fusion at two developmental stages

A and *B*, presynaptic $[Ca^{2+}]_i$ steps produced by Ca^{2+} uncaging with different UV light intensities (*A*) and the resulting EPSCs in the postsynaptic cell (*B*), for recordings in a P9 rat (left) and a P14 rat (right). The insets in *B* show transmitter release rates as obtained by EPSC deconvolution. *C*, plot of the peak release rates as a function of the corresponding $[Ca^{2+}]_i$ steps on double-logarithmic coordinates. The values for $[Ca^{2+}]_i$ steps below 10 μM amplitude were fitted by lines. The data obtained from the example cells (*A* and *B*) are shown by black symbols and lines; data points and fits for all other cells obtained with 2 mM DM-nitrophen are shown by grey symbols and lines. *D*, average slope values derived from fitting the peak release rate–$[Ca^{2+}]_i$ relation (see *C*). There was no significant change ($P = 0.49$), indicating that the intrinsic Ca^{2+} cooperativity of release was unchanged during development. *E*, plot of the average interpolated $[Ca^{2+}]_i$ value needed to evoke a peak transmitter release rate of 100 ves ms^{-1} (at P8–P9), or a pool-corrected value of 160 ves ms^{-1} at P12–P15 group (dashed lines in *C*). There was a 1.29-fold increase of this $[Ca^{2+}]_i$ value, indicating a slightly lower Ca^{2+} sensitivity with development ($P = 0.012$).

pairs in each age group (see Fig. 3*C*, grey symbols and fit lines), we found average intrinsic Ca^{2+} cooperativities of release of 3.5 ± 0.3 at P8–P9 ($n = 8$ cell pairs with 2 mM presynaptic DM-nitrophen) and 3.7 ± 0.2 at P12–P15 ($n = 10$ cell pairs; $P = 0.49$; Fig. 3*D*). Thus, there was no measurable change in the intrinsic Ca^{2+} cooperativity of transmitter release with development.

As a first estimate for the intrinsic Ca^{2+} sensitivity of release, we computed, using linear regression of the data points, the post-flash $[Ca^{2+}]_i$ value that was necessary to trigger a given value of peak transmitter release rate. We used an arbitrary reference value of 100 vesicles (ves) ms^{-1} for the age group of P8–P9 (Fig. 3*C*, left panel). This value was scaled to 160 ves ms^{-1} for the age group of P12–P15 (Fig. 3*C*, right panel), since the pool of fast-releasable vesicles, which underlies the peak release rates measured after Ca^{2+} uncaging, was increased by about 1.6-fold with development (see below; Fig. 4). The corresponding interpolated post-flash $[Ca^{2+}]_i$ values were 4.9 ± 0.4 μM at P8–P9 ($n = 8$ cell pairs) and 6.3 ± 0.4 μM at P12–P15 ($n = 10$ cell pairs; $P = 0.012$; Fig. 3*E*). Thus, a somewhat higher post-flash $[Ca^{2+}]_i$ was needed in the more mature synapses to evoke a peak release rate of the same (pool-corrected) amplitude. This difference suggests that the intracellular Ca^{2+} sensitivity of vesicle fusion might be slightly reduced with development, as found recently in mice (Wang *et al.* 2008). We will address this possibility in more detail below (see Fig. 5).

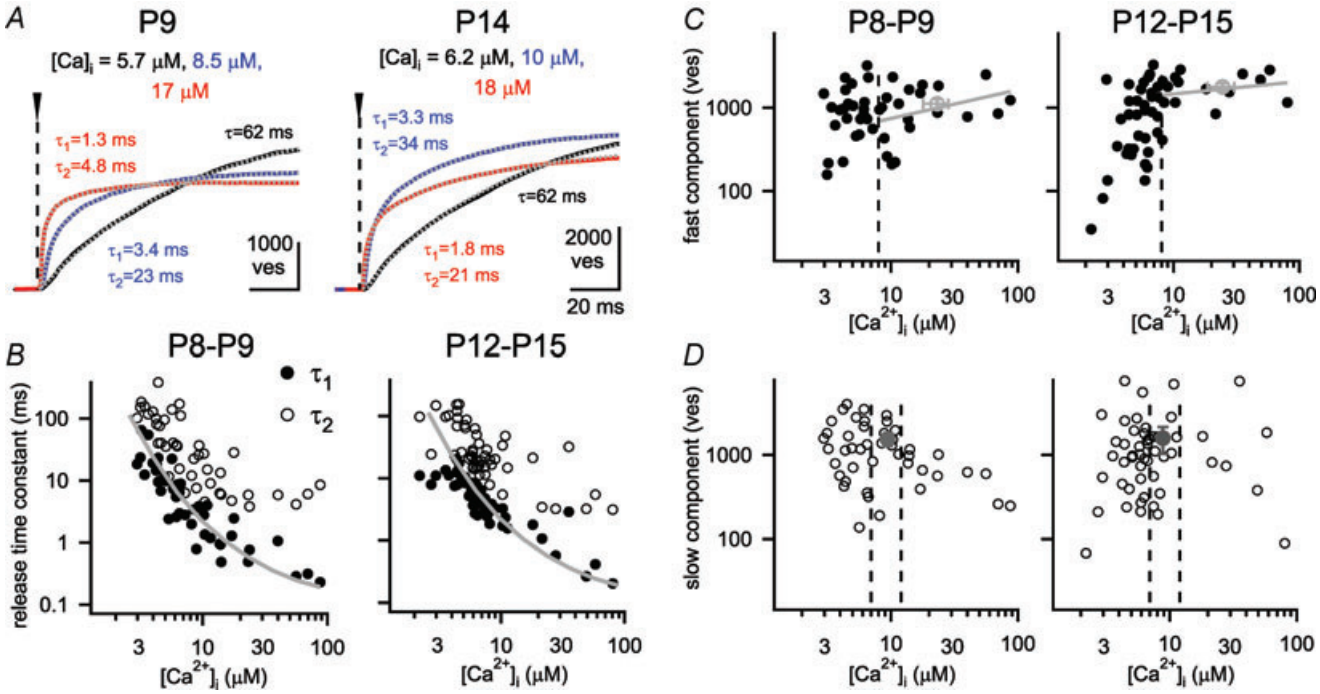

Figure 4. Ca^{2+} uncaging evokes a fast and a slow component of transmitter release at both developmental stages

A, integrated release rate traces for a P9 (left) and a P14 (right) synapse evoked by step-like elevations of $[Ca^{2+}]_i$ (traces are from the same cells and in colours corresponding to the examples shown in Fig. 3*A* and *B*). The post-flash $[Ca^{2+}]_i$ value for each response is indicated. The cumulative release rate traces were fitted with various exponential fit functions (see Methods), and the best-fit traces are shown superimposed (grey dotted lines): single exponentials for the lowest $[Ca^{2+}]_i$ steps (black traces, time constant τ indicated), or double exponentials, with the indicated values for τ_1 and τ_2. *B*, the two time constants (τ_1 and τ_2) of the fast and the slow release component were plotted against the corresponding post-flash $[Ca^{2+}]_i$ values at P8–P9 (left panel) and at P12–P15 (right panel). The prediction of the five-site model of Ca^{2+} binding and vesicle fusion, which effectively models the fast release component, is superimposed (grey line; parameters as given for the P8–P9 age group in the legend to Fig. 5). Note that this data set, and the data shown in *C* and *D* also include experiments done with 5 mM DM-nitrophen, which allowed us to obtain higher post-flash $[Ca^{2+}]_i$ values of up to 90 μM. *C* and *D*, the number of vesicles released in each kinetic component of release as a function of post-flash $[Ca^{2+}]_i$, plotted separately for P8–P9 (left panels) and for P12–P15 rats (right panels). The numbers were estimated by the amplitude values of the fast and the slow time constants in fits of the cumulative release rate traces (*A* and *B*), when the best-fit functions were either double-exponentials, double-exponentials plus line, or triple exponential functions. The average number of vesicles released in the fast component by $[Ca^{2+}]_i$ steps above 8 μM is indicated by the grey average symbol. For $[Ca^{2+}]_i > 8$ μM, the data for the fast release component were fitted by lines (grey lines in *C*). The average number of slowly released vesicles was estimated in the $[Ca^{2+}]_i$ range of 7–12 μM (see dotted lines and grey average symbols in *D*), because the number of slowly released vesicles showed a tendency to decrease with $[Ca^{2+}]_i$ steps > 15 μM.

Ca^{2+} uncaging evokes two components of transmitter release at both developmental stages

It has been shown previously in calyces of Held of young rats (P8–P10) that long voltage-clamp depolarizations of 30–50 ms lengths induce two phases of release that are mediated by fast- and slowly releasable vesicle sub-pools (Sakaba & Neher, 2001). Similarly, Ca^{2+} uncaging stimuli caused two kinetically separate components of transmitter release (Wölfel *et al.* 2007). This suggested that an intrinsic mechanism, such as different Ca^{2+} sensitivities, underlies the separation between fast- and slowly releasable vesicles (Wölfel *et al.* 2007; but see Wadel *et al.* 2007). It is possible, however, that the slow transmitter release phase could be a hallmark of the relatively young synapses studied previously, and that developmental maturation leads to a suppression of the slow release mechanism (see Price & Trussell, 2007). In order to investigate this possibility, we next analysed the kinetics of transmitter release evoked by Ca^{2+} uncaging at the two developmental stages, by integrating the transmitter release rate traces obtained from EPSC deconvolution (Fig. 4).

Figure 4*A* shows the integrated release rate traces for the same cells that are illustrated in Fig. 3*A* and *B* (with an identical colour code). These traces of cumulative release were best fitted by functions with at least two exponential terms for the higher $[Ca^{2+}]_i$ steps (Fig. 4*A*, red and blue traces; see Methods for details of determining the best-fit function). On the other hand, cumulative release traces in response to $[Ca^{2+}]_i$ steps of lower amplitude were often well fitted by a single exponential term (Fig. 4*A*, black traces). When the resulting release time constants were plotted as a function of $[Ca^{2+}]_i$ (Fig. 4*B*), both the fast and the slow release time constants were found to be strongly $[Ca^{2+}]_i$ dependent (Fig. 4*B*; Wölfel *et al.* 2007). The inverse dependence on the $[Ca^{2+}]_i$ of both release time constants was highly significant at each developmental stage (Pearson's test; $P < 10^{-8}$). When the fast release time constants for each developmental stage were overlaid, it became apparent that they were indistinguishable (see Supplemental Fig. 1*A*).

We next analysed the amounts of fast and slowly released vesicles as a function of $[Ca^{2+}]_i$ (Fig. 4*C* and *D*). At post-flash $[Ca^{2+}]_i > 8\ \mu M$, a near-maximal number of vesicles was released in the fast release component (Fig. 4*C*), although there was a slight tendency towards larger cumulative fast release at $[Ca^{2+}]_i$ values beyond $10\ \mu M$ (Fig. 4*C*, grey fit lines; see also Wölfel *et al.* 2007). We assumed that flashes that elevated $[Ca^{2+}]_i$ to values of $8\ \mu M$ or higher deplete the pool of fast-releasable vesicles as shown before (Schneggenburger & Neher, 2000). Therefore, we took the amplitude of the fast release component in response to flashes that elevated $[Ca^{2+}]_i$ above $8\ \mu M$ as an estimate of the size of the fast-releasable pool. This number was 1109 ± 153 vesicles at P8–P9 ($n = 10$ cell pairs) and 1767 ± 194 vesicles at P12–P15 ($n = 8$ cell pairs; see Fig. 4*C*, grey average data points). The number of vesicles released in the slow component with $[Ca^{2+}]_i$ steps in the range of 7–12 μM was 1542 ± 268 at P8–P9 and 1586 ± 582 at P12–P15 (Fig. 4*D*, grey data points). With $[Ca^{2+}]_i$ steps of larger amplitudes, the number of vesicles released in the slow component showed a tendency to decrease, similar to previous findings in young calyces of Held (Wölfel *et al.* 2007).

Taken together, the kinetic analysis of transmitter release evoked by Ca^{2+} uncaging shows clearly separable fast and slow release components after Ca^{2+} uncaging, as observed before in young rats (Wölfel *et al.* 2007). This indicates that a mechanism intrinsic to the release machinery is responsible for generating fast and slow release, like the existence of fast- and slowly releasable vesicle sub-pools (FRPs and SRPs) with different effective Ca^{2+} sensitivities of release (Voets, 2000; Wölfel *et al.* 2007; but see Wadel *et al.* 2007). Second, the data also show that with development, the intrinsically slow release component persists, and that the size of the FRP increases with development.

Nearly unchanged intrinsic Ca^{2+} sensitivity of transmitter release with developmental maturation

We next wished to fit the Ca^{2+} dependence of transmitter release with a simple model of Ca^{2+} binding and vesicle fusion, the five-site model (Schneggenburger & Neher, 2000). The parameters of the fit can subsequently be used to back-calculate, for each developmental stage, the 'local' $[Ca^{2+}]_i$ signal that a given readily releasable vesicle might experience during the physiological release response (Schneggenburger & Neher 2005). For fitting the model to the Ca^{2+} uncaging data, we simultaneously fitted the $[Ca^{2+}]_i$ dependencies of the peak release rate, the release delay and the time to peak release rate (Fig. 5*Aa*, *B* and *C*). These three parameters should primarily reflect release from the fast-releasable vesicle sub-pool, since the initial peak in the transmitter release rate after Ca^{2+} uncaging is carried by fast-releasable vesicles (Wölfel *et al.* 2007). Thus, fitting these parameters with the five-site model of Ca^{2+} binding and vesicle fusion will essentially model release from the FRP only. This is justified, because for the back-calculation of the local $[Ca^{2+}]_i$ transient that drives the fast phase of transmitter release during a presynaptic AP (see below; Fig. 6), only fast-releasable vesicles are relevant, since AP-evoked release is carried by FRP vesicles (Sakaba, 2006).

Figure 5 shows the $[Ca^{2+}]_i$ dependencies of the transmitter release rates (Fig. 5*Aa*), the release delays (Fig. 5*B*) and the time to peak release rates (Fig. 5*C*), as well as the resulting fit predictions. Overall, the data from the two developmental groups overlaid markedly

well, indicating that there was no major change in the intrinsic Ca^{2+} sensitivity of vesicle fusion. The values of the resulting fit parameters (see legend for Fig. 5) indicated a ratio of k_{off}/k_{on} of 54 μM in the young age group and 69 μM in the more mature age group, which might indicate a slight rightward shift of the release rate *versus* post-flash $[Ca^{2+}]_i$ relation. Figure 5*Ab* shows a plot of pool-normalized peak release rates (normalized by the size of the FRP estimated in each cell), with the pool-normalized fit predictions overlaid (these were normalized to the corresponding average FRP size at each developmental stage; 1109 and 1767 vesicles at P8–P9 and at P12–P15, respectively; see above, Fig. 4*C*). In this pool-corrected plot, the fit lines illustrate more clearly the slight rightward shift of the more mature age group with respect to the younger age group (Fig. 5*Ab*; black and grey line, respectively). Note, however, that the scatter of the data within each age group is larger than the difference between the fit predictions for each age group (see also Supplemental Fig. 2). This suggests that the slight, about 1.3-fold rightward shift in the $[Ca^{2+}]_i$ sensitivity of release found by fitting the data is not highly significant. It should also be noted that the $[Ca^{2+}]_i$ dependency of the release delays was unchanged between the two age groups (Fig. 5*B*). The $[Ca^{2+}]_i$ dependency of the time to peak release was more shallow in the age group of P12–P15 than at P8–P9 especially at low $[Ca^{2+}]_i$ (Fig. 5*C*), but this tendency was not captured by the model fit.

In conclusion, the drastic leftward shift in the relation between EPSCs and presynaptic Ca^{2+} current charge (Q_{Ca}; Figs 1 and 2) cannot be explained by a change in the intrinsic Ca^{2+} sensitivity of vesicle fusion. On the contrary, there might be a slight, ~1.3-fold *decrease* in the intracellular Ca^{2+} sensitivity of vesicle fusion upon developmental maturation of the presynaptic transmitter release machinery. This agrees with the recent report of Wang *et al.* (2008), who found an ~1.5-fold rightward shift of the $[Ca^{2+}]_i$ dependency of peak transmitter release, studying developmental maturation in the mouse calyx of Held. Taken together, the pronounced, ~1.6- to 2-fold leftward shift in the EPSCs–Q_{Ca} relation that we found here (Figs 1 and 2) is therefore most probably caused by a tighter co-localization of Ca^{2+} channels and readily releasable vesicles (Fedchyshyn & Wang, 2005).

The local $[Ca^{2+}]_i$ signal seen by a readily releasable vesicle is increased during development

A likely consequence of the postulated tighter co-localization of readily releasable vesicles with Ca^{2+} channels is that vesicles would experience a higher local $[Ca^{2+}]_i$ signal. To investigate this possibility, we next measured EPSCs evoked by presynaptic APs at each developmental stage, with the aim to back-calculate the local $[Ca^{2+}]_i$ transient at each developmental stage. We recorded EPSCs in response to afferent fibre stimulation at the two age groups, in the presence of CTZ (100 μM). Two example average EPSC traces for one cell of each age group are shown in Fig. 6*A*. The EPSC amplitudes in these cells were 10.6 nA and 8.4 nA, and among all the

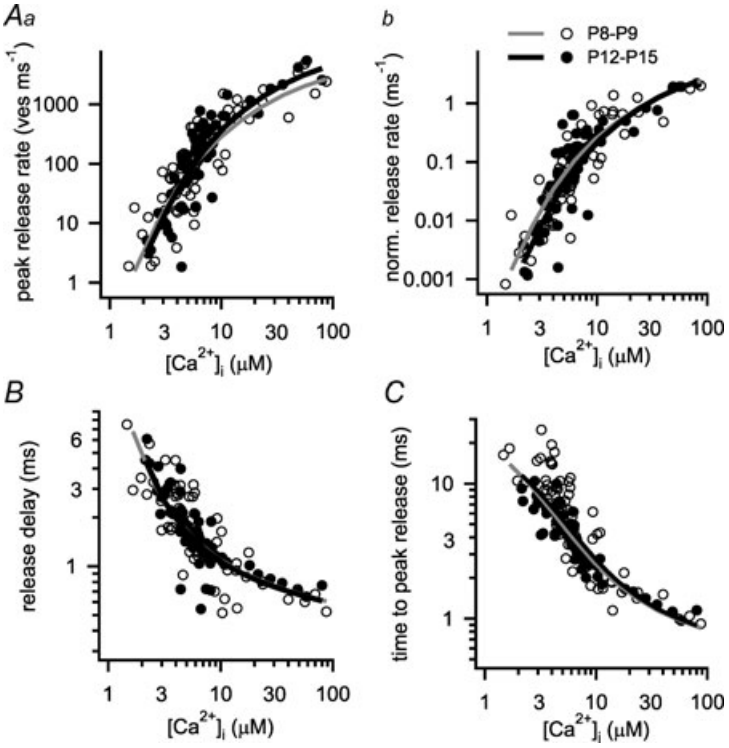

Figure 5. The intrinsic Ca^{2+} sensitivity of transmitter release is largely unchanged during developmental refinement of synaptic transmission
A–C, plots of the peak transmitter release rates (*Aa*), the pool-corrected peak release rate (*Ab*), the minimal release delay (*B*), and the time to the peak of the transmitter release rate (*C*) as a function of presynaptic $[Ca^{2+}]_i$ reached after flashes for both developmental groups (P8–P9, open symbols; P12–P15, filled symbols). In *Ab*, the peak release rates were normalized by the pool size estimate (FRP) of each individual cell. The data points for the two developmental groups largely overlap for all analysed parameters. The data sets in *Aa*, *B* and *C* were simultaneously fitted with the five-site model of cooperative Ca^{2+} binding and vesicle fusion (Schneggenburger & Neher, 2000), yielding the following parameters for each age group: $k_{on} = 1.21 \times 10^8$ M^{-1} s^{-1}, $k_{off} = 6500$ s^{-1}, $b = 0.26$, $\gamma = 6960$ s^{-1} (P8–P9 age group; grey fit lines); and $k_{on} = 1.15 \times 10^8$ M^{-1} s^{-1}, $k_{off} = 7900$ s^{-1}, $b = 0.26$, $\gamma = 6960$ s^{-1} (P12–P15 age group; black fit lines). In *Ab*, the fit predictions were normalized by the average FRP pool size values obtained in young synapses (1109 vesicles; P8–P9) and in more mature synapses (1767 vesicles; see Results). A small, constant delay (0.4 ms) was added to the model predictions of release delay (*B*) and time to peak release (*C*), indicating a time delay not explained by the model (see also Bollmann *et al.* 2000; Felmy *et al.* 2003).

cells the average EPSC amplitudes were 11.7 ± 2.0 nA at P8–P9 ($n = 6$ cells) and 10.3 ± 1.1 nA at P12–P15 ($n = 6$ cells), not significantly different ($P = 0.52$). Despite the unchanged average EPSC amplitude, the EPSC rise time was significantly shorter in older animals (199 ± 11 μs at P12–P15, $n = 6$ cells) than in the younger age group (309 ± 9 μs at P8–P9; $n = 6$ cells; $P < 0.001$). Similarly, the release rates obtained by EPSC deconvolution (Fig. 6*B*) were significantly briefer in the more mature animals, with half-widths of 443 ± 14 μs at P8–P9 and 326 ± 19 μs at P12–P15 ($n = 6$ cells each; $P < 0.001$; Fig. 6*D*, right panel). This indicates that transmitter release occurs over a briefer time window in more mature animals (Taschenberger *et al.* 2005).

We next back-calculated the 'local' $[Ca^{2+}]_i$ signal that an average readily releasable vesicle might experience at each developmental stage (Fig. 6*C*). Note that this back-calculation has no free parameters except the timing and the amplitude parameters of the 'local' $[Ca^{2+}]_i$ signal to be found (see Methods); the parameters that describe the Ca^{2+} sensitivity of vesicle fusion at each developmental stage have been fixed beforehand by fitting the five-site model to the Ca^{2+} uncaging data (Fig. 5). For the two example synapses shown in Fig. 6*A* and *B*, the back-calculated local $[Ca^{2+}]_i$ signal had amplitudes of 26 μM and 36 μM with half-widths of 432 μs and 287 μs in a P8 and a P14 synapse, respectively (Fig. 6*C*). On average, the local $[Ca^{2+}]_i$ transient significantly increased with maturation, from a value of 27.5 ± 1.1 μM at P8–P9 ($n = 6$ cells) to 35.1 ± 2.2 μM at P12–P15 ($n = 6$ cells; $P = 0.009$; Fig. 6*E*, left panel). At the same time, the back-calculated local $[Ca^{2+}]_i$ signal was significantly briefer at P12–P15 (half-width, 320 ± 23 μs) as compared to P8–P9 (481 ± 18 μs; $P < 0.001$; Fig. 6*E*, right panel). Since the amount of transmitter release depends on the amplitude of the local $[Ca^{2+}]_i$ signal (power function with exponent of about 4) as well as on its width (power function with exponent of $\sim$1.5; Bollmann & Sakmann, 2005), it is likely that the effects on release of a $\sim$1.3-fold larger, but $\sim$1.5-fold briefer local $[Ca^{2+}]_i$ signal roughly compensate each other. This would explain the similar EPSC amplitudes observed at both developmental stages in rats (see above, Fig. 6*A*; Taschenberger & von Gersdorff, 2000; Iwasaki & Takahashi, 2001).

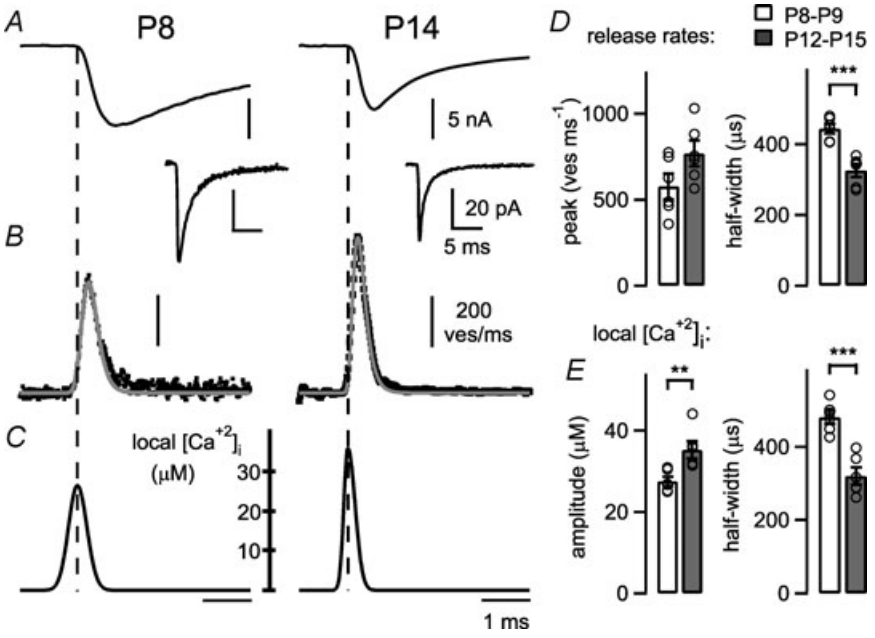

Figure 6. The 'local' $[Ca^{2+}]_i$ signal experienced by readily releasable vesicles during AP-evoked release increases with development

A, EPSCs (average of $n = 5$ traces each) evoked by afferent fibre stimulation in a P8 and a P14 synapse, in the presence of cyclothiazide (CTZ). The average mEPSC waveform recorded in each cell is also shown (lower trace; note different scales). *B*, transmitter release rates (average of $n = 5$ single sweeps; black data points) for the EPSCs shown in *A*, as obtained by deconvolution of the evoked EPSC with the mEPSC waveform (see Methods). The transmitter release rates predicted by the 'local' $[Ca^{2+}]_i$ waveforms shown in *C* are superimposed (grey traces). *C*, the iteratively refined local $[Ca^{2+}]_i$ waveforms which best predicted the observed transmitter release rates shown in *B*. *D*, average peak transmitter release rates (left) and their half-widths (right) for each developmental stage. Note the highly significant ($P < 0.001$) reduction in the half-width of AP-evoked transmitter release with development (right panel). *E*, average amplitude (left) and half-widths (right) of the back-calculated local $[Ca^{2+}]_i$ transients for both developmental stages. Note that the local $[Ca^{2+}]_i$ signal is significantly higher ($P = 0.009$, left), and at the same time briefer in more mature animals ($P < 0.001$, right).

The shorter duration of the local $[Ca^{2+}]_i$ signal that we derived in Fig. 6 most likely reflects a shortening of the duration of the presynaptic AP that has been observed with developmental maturation at the calyx of Held (Taschenberger & von Gersdorff, 2000; Yang & Wang, 2006). A briefer presynaptic AP would lead to a shorter presynaptic Ca^{2+} current and thereby to a briefer local $[Ca^{2+}]_i$ transient, as found here by the back-calculation approach (Fig. 6). To investigate this possibility, we measured presynaptic APs, and performed a Hodgkin–Huxley simulation of the presynaptic Ca^{2+} current induced by these APs at P8–P9 and at P12–P15 (see Supplemental Fig. 3). The simulations showed that the Ca^{2+} current is expected to be about 2-fold faster in the more mature synapses than at the younger age group (Supplemental Fig. 3). This suggests that the changes in the timing of the 'local' $[Ca^{2+}]_i$ signal with development (Fig. 6*C* and *E*) can be well explained by the briefer AP in the nerve terminal. On the other hand, the increased amplitude of the local $[Ca^{2+}]_i$ signal probably indicates a tighter co-localization of Ca^{2+} channels and readily releasable vesicles (see Discussion).

Discussion

We have investigated the presynaptic mechanisms underlying the developmental enhancement of Ca^{2+}–secretion coupling at the calyx of Held of rats. We found an about 2-fold leftward shift in the relationship between EPSC amplitudes and the presynaptic Ca^{2+} current charge (Figs 1 and 2), indicating a significant increase in the efficiency of brief Ca^{2+} currents in evoking release. Despite this pronounced leftward shift, Ca^{2+} uncaging experiments revealed a nearly constant, or even slightly rightward-shifted intrinsic Ca^{2+} sensitivity of transmitter release (Figs 3–5). This strongly suggests that the increased efficiency of brief Ca^{2+} currents in evoking transmitter release (Taschenberger *et al.* 2002; Fedchyshyn & Wang, 2005) is caused by a tighter Ca^{2+} channel–vesicle co-localization. A back-calculation of the 'local' $[Ca^{2+}]_i$ signal based on the intracellular Ca^{2+} sensitivities of transmitter release at each developmental stage showed that an average readily releasable vesicle experiences a local $[Ca^{2+}]_i$ signal with an about 30% increased amplitude upon developmental maturation (Fig. 6). This provides independent evidence for the idea that the Ca^{2+} channel–vesicle co-localization becomes tighter with development at the calyx of Held (Fedchyshyn & Wang, 2005).

Developmental changes in the intrinsic Ca^{2+} sensitivity of vesicle fusion

We used presynaptic Ca^{2+} uncaging to study possible developmental changes in the intracellular Ca^{2+} sensitivity of vesicle fusion during development. We found an overall very similar $[Ca^{2+}]_i$-dependent regulation of transmitter release at both developmental stages studied here. Thus, the peak release rates were steeply dependent on the post-flash $[Ca^{2+}]_i$ with identical slopes (Figs 3*C* and 5*A*), indicating no change in the intrinsic ('biochemical') Ca^{2+} cooperativity of release. In addition, the $[Ca^{2+}]_i$-dependent release delays were unchanged (Fig. 5*B*). Furthermore, we found that at both developmental stages, release evoked by Ca^{2+} uncaging showed two distinct kinetic phases (Fig. 4), confirming earlier findings made in young calyces of Held (Wölfel *et al.* 2007). Since Ca^{2+} uncaging induces a spatially homogeneous $[Ca^{2+}]_i$ signal (Naraghi *et al.* 1998; Wölfel *et al.* 2007), the observation of two kinetically distinct release components indicates that the separation between the fast and the slow release components is caused by a mechanism intrinsic to the release machinery. As a working hypothesis for this intrinsic heterogeneity, we assume that the total readily releasable pool is sub-divided into a fast- and a more slowly releasable sub-pool (FRP and SRP, respectively), which have distinct intrinsic Ca^{2+} sensitivities (Voets, 2000; Wölfel *et al.* 2007). Adaptation of the vesicle fusion machinery to Ca^{2+} (Hsu *et al.* 1996) has also been considered as a mechanism of intrinsic heterogeneity of release kinetics (Wölfel *et al.* 2007). Regardless of the exact explanation, the persistence of a slow release component after Ca^{2+} uncaging in more mature synapses indicates that the intrinsic propensity for slow transmitter release is maintained during development.

The number of vesicles released in the fast release component with $[Ca^{2+}]_i$ steps above 8 μM increased by ~1.6-fold, indicating an increase of the FRP with development (Fig. 4*C*). This increase in the fast-releasable pool probably corresponds to the developmental pool size increase that was found previously by analysing cumulative peak EPSC amplitudes during 100 Hz trains (Iwasaki *et al.* 2000; Taschenberger & von Gersdorff, 2000), since the phasic release during AP-evoked EPSCs is carried by fast-releasable vesicles (Sakaba, 2006). When we normalized the measured absolute peak release rates by the FRP size determined in each synapse, a slight, ~1.3-fold rightward shift of the peak release rate became apparent (Fig. 5*Ab*). Similarly, a (pool-corrected) reference release rate was only reached at an ~1.3-fold higher post-flash $[Ca^{2+}]_i$ in the more mature synapses (Fig. 3*C*). Both findings are consistent with the recent report of an about 1.5-fold rightward shift of the intrinsic Ca^{2+} sensitivity of transmitter release in mice (Wang *et al.* 2008); the more pronounced rightward shift in the previous study is probably explained by the use of older animals in the more mature age group (P16–P19 mice). Together, the present study, and the recently published work by Wang *et al.* (2008) show that changes

in the intrinsic Ca^{2+} sensitivity of vesicle fusion cannot explain the increased efficiency of brief Ca^{2+} currents in evoking release (Figs 1 and 2; and see Taschenberger *et al.* 2002; Fedchyshyn & Wang, 2005). These findings from Ca^{2+} uncaging experiments present significant new evidence in support of the hypothesis that the spatial coupling between Ca^{2+} channels and vesicles is enhanced during developmental maturation (Fedchyshyn & Wang, 2005).

Increased release efficiency of brief presynaptic Ca^{2+} currents with development

Previous work has shown a developmental decrease in the Ca^{2+} current–release cooperativity at the mouse calyx of Held (Fedchyshyn & Wang, 2005), but there was little emphasis on the release efficiency of brief Ca^{2+} currents on an absolute scale. Here, we found that brief presynaptic Ca^{2+} currents become significantly more efficient in triggering transmitter release, as manifested by a clear, 1.6- to 2-fold leftward shift in double-logarithmic plots of the EPSC amplitude *versus* presynaptic Ca^{2+} charge (Q_{Ca}; Figs 1 and 2). When release was evoked by brief presynaptic Ca^{2+} tail currents, we found a slight decrease in the Ca^{2+} current–release cooperativity with development, in addition to the clear, ∼1.6-fold leftward shift on the Q_{Ca} axis (Fig. 2). Although the change in Ca^{2+} current–release cooperativity was smaller than what was previously found in mice, the trend in our data confirms the previous study (Fedchyshyn & Wang, 2005), and indicates that fewer Ca^{2+} channels are involved in the release control of a given readily releasable vesicle (see Discussion below). With depolarizing steps to 0 mV there was no measurable change in the steepness of the EPSC–Q_{Ca} relationship (Fig. 1). This might have been caused by the confounding effects of the Ca^{2+} charge that enters the nerve terminal during the pulse to 0 mV, which is probably less efficient in triggering release as compared to the larger Ca^{2+} tail currents.

The leftward shift in the EPSC–Q_{Ca} relationship probably represents a tighter spatial coupling between Ca^{2+} channels and vesicles localized within each active zone. Two alternative explanations need to be considered, though. First, the increased size of the FRP (∼1.6-fold; Fig. 4*C*) could contribute to an apparent leftward shift of the EPSC–Q_{Ca} relationship. However, given the steep relationship between EPSC amplitudes and Q_{Ca} (slopes of ∼3.5 in the double-logarithmized data sets), a 2-fold leftward shift of the EPSC–Q_{Ca} relation corresponds to an about 10-fold increased transmitter release at any given Q_{Ca} value (see also Figs 1*C* and 2*C*; left vertical dashed line). Therefore, the ∼1.6-fold increased FRP size should contribute only by a small degree to the observed leftward shift of the EPSC–Q_{Ca} data. Second, a reduced endogenous Ca^{2+} buffering strength could, in principle, also contribute to a higher efficiency of presynaptic Ca^{2+} entry in evoking release. However, the available evidence indicates that the Ca^{2+} buffering strength of the calyx of Held *increases* with development (Chuhma *et al.* 2001; Felmy & Schneggenburger, 2004), making decreased Ca^{2+} buffering an unlikely explanation.

It is currently not known which fraction of the measured presynaptic Ca^{2+} current corresponds to Ca^{2+} channels located at the active zone. For many CNS synapses, including the calyx of Held, immunogold EM analysis of the presynaptic localization of P/Q-type Ca^{2+} channels is not yet available (but see Bucurenciu *et al.* 2008). At the calyx of Held, there is also a developmental down-regulation of presynaptic N- and R-type Ca^{2+} channels (Wu *et al.* 1999), such that at ∼P12–P14 a majority of the presynaptic Ca^{2+} channels are of the P/Q subtype (Iwasaki *et al.* 2000). This re-organization of voltage-gated Ca^{2+} channel subtypes might go along with a change in the fraction of Ca^{2+} channels located at active zones. Despite this possibility, the simplest explanation for the pronounced leftward shift in the EPSC–Q_{Ca} relationship is to assume that a significantly smaller Ca^{2+} current at each active zone is sufficient to cause a given rate of transmitter release in more mature calyces of Held.

Implications for Ca^{2+} signalling at single active zones

What are the consequences of these developmental changes for Ca^{2+} signalling at single active zones? If one assumes, for the purpose of this argument, that during development the total number of Ca^{2+} channels stays constant at each active zone, then the integral Ca^{2+} influx at each active zone would be reduced by about 50%, because of the significant developmental shortening of the AP duration (Supplemental Fig. 3; Yang & Wang, 2006). Part of the reduced Ca^{2+} entry is probably caused by the opening of fewer Ca^{2+} channels, and another part by the shorter duration of current flow through individual channels (see Supplemental Fig. 3). Without a tighter co-localization, as suggested previously by the decreased efficiency of EGTA in suppressing release (Fedchyshyn & Wang, 2005), a 2-fold reduction of the Ca^{2+} influx at an active zone would lead to a strong reduction of release probability, which is not observed. On the contrary, we found that the back-calculated 'local' $[Ca^{2+}]_i$ became significantly higher by ∼30% with development; at the same time, however, the width of the local $[Ca^{2+}]_i$ signal was decreased, reflecting a briefer Ca^{2+} current in response to briefer APs (Fig. 6; Supplemental Fig. 3). Very similar findings were reported recently for the developing mouse calyx of Held (Wang *et al.* 2008). This increase in the peak amplitude of the local $[Ca^{2+}]_i$ signal is consistent with the idea that the Ca^{2+} channel–vesicle co-localization

becomes tighter in development (Fedchyshyn & Wang, 2005). The alternative explanation of an increased Ca^{2+} channel density around a docked vesicle is unlikely because the decreased Ca^{2+} current–release cooperativity suggests that fewer Ca^{2+} channels contribute to the release control of a given vesicle.

Taken together, the developmental changes in Ca^{2+} signalling during a presynaptic AP at the calyx of Held are dictated by the shorter presynaptic AP and, as a consequence, by a briefer Ca^{2+} current. Nevertheless, the 'local' $[Ca^{2+}]_i$ signal is enhanced because of a tighter co-localization of probably fewer (open) Ca^{2+} channels with a given readily releasable vesicle. An active zone contains 3–5 docked vesicles and it is likely that each docked vesicle is quite tightly coupled to several Ca^{2+} channels. Thus, the co-localization of docked vesicles and Ca^{2+} channels in the active zone is probably not random, but a higher local density of Ca^{2+} channels must exist around docked vesicles. How this process of docking and positioning close to Ca^{2+} channels is molecularly coordinated is currently unknown. A tight molecular interaction between Ca^{2+} channels and vesicles can be mediated by SNARE proteins and Ca^{2+} channels via their 'Synprint' site (Sheng *et al.* 1994; Rettig *et al.* 1996), but such a tight molecular coupling may not explain the entire complexity of docked vesicle–Ca^{2+} channel co-localization. Alternatively or additionally, presynaptic scaffolding- and organizing-molecules such as the Rab-interacting molecules (Rims) could be involved in mediating co-localization, since these molecules probably integrate functions in vesicle docking and priming (Kaeser & Sudhof, 2005) with direct or indirect interaction with Ca^{2+} channels at the active zone (Hibino *et al.* 2002; Kiyonaka *et al.* 2007).

References

Augustine GJ, Adler EM & Charlton MP (1991). The calcium signal for transmitter secretion from presynaptic nerve terminals. *Ann N Y Acad Sci* **635**, 365–381.

Bollmann JH & Sakmann B (2005). Control of synaptic strength and timing by the release-site Ca^{2+} signal. *Nat Neurosci* **8**, 426–434.

Bollmann JH, Sakmann B & Borst JG (2000). Calcium sensitivity of glutamate release in a calyx-type terminal. *Science* **289**, 953–957.

Borst JG & Sakmann B (1998). Calcium current during a single action potential in a large presynaptic terminal of the rat brainstem. *J Physiol* **506**, 143–157.

Borst JG & Sakmann B (1999). Effect of changes in action potential shape on calcium currents and transmitter release in a calyx-type synapse of the rat auditory brainstem. *Philos Trans R Soc Lond B Biol Sci* **354**, 347–355.

Brandt A, Khimich D & Moser T (2005). Few $Ca_V1.3$ channels regulate the exocytosis of a synaptic vesicle at the hair cell ribbon synapse. *J Neurosci* **25**, 11577–11585.

Bucurenciu I, Kulik A, Schwaller B, Frotscher M & Jonas P (2008). Nanodomain coupling between Ca^{2+} channels and Ca^{2+} sensors promotes fast and efficient transmitter release at a cortical GABAergic synapse. *Neuron* **57**, 536–545.

Chuhma N, Koyano K & Ohmori H (2001). Synchronisation of neurotransmitter release during postnatal development in a calyceal presynaptic terminal of rat. *J Physiol* **530**, 93–104.

Fedchyshyn MJ & Wang LY (2005). Developmental transformation of the release modality at the calyx of Held synapse. *J Neurosci* **25**, 4131–4140.

Felmy F, Neher E & Schneggenburger R (2003). The timing of phasic transmitter release is Ca^{2+} dependent and lacks a direct influence of presynaptic membrane potential. *Proc Natl Acad Sci U S A* **100**, 15200–15205.

Felmy F & Schneggenburger R (2004). Developmental expression of the Ca^{2+}-binding proteins calretinin and parvalbumin at the calyx of Held of rats and mice. *Eur J Neurosci* **20**, 1473–1482.

Futai K, Okada M, Matsuyama K & Takahashi T (2001). High-fidelity transmission acquired via a developmental decrease in NMDA receptor expression at an auditory synapse. *J Neurosci* **21**, 3342–3349.

Geal-Dor M, Freeman S, Li G & Sohmer H (1993). Development of hearing in neonatal rats: air and bone conducted ABR thresholds. *Hear Res* **69**, 236–242.

Gentile L & Stanley EF (2005). A unified model of presynaptic release site gating by calcium channel domains. *Eur J Neurosci* **21**, 278–282.

Hibino H, Pironkova R, Onwumere O, Vologodskaia M, Hudspeth AJ & Lesage F (2002). RIM binding proteins (RBPs) couple Rab3-interacting molecules (RIMs) to voltage-gated Ca^{2+} channels. *Neuron* **34**, 411–423.

Hoffpauir BK, Grimes JL, Mathers PH & Spirou GA (2006). Synaptogenesis of the calyx of Held: Rapid onset of function and one-to-one morphological innervation. *J Neurosci* **26**, 5511–5523.

Hsu S-F, Augustine GJ & Jackson MB (1996). Adaptation of Ca^{2+}-triggered exocytosis in presynaptic terminals. *Neuron* **17**, 501–512.

Iwasaki S, Momiyama A, Uchitel OD & Takahashi T (2000). Developmental changes in calcium channel types mediating central synaptic transmission. *J Neurosci* **20**, 59–65.

Iwasaki S & Takahashi T (2001). Developmental regulation of transmitter release at the calyx of Held in rat auditory brainstem. *J Physiol* **534**, 861–871.

Jewett DL & Romano MN (1972). Neonatal development of auditory system potentials averaged from the scalp of rat and cat. *Brain Res* **36**, 101–115.

Joshi I & Wang L-Y (2002). Developmental profiles of glutamate receptors and synaptic transmission at a single synapse in the mouse auditory brainstem. *J Physiol* **540**, 861–873.

Kaeser PS & Sudhof TC (2005). RIM function in short- and long-term synaptic plasticity. *Biochem Soc Trans* **33**, 1345–1349.

Kandler K & Friauf E (1993). Pre- and postnatal development of efferent connections of the cochlear nucleus in the rat. *J Comp Neurol* **328**, 161–184.

Kiyonaka S, Wakamori M, Miki T, Uriu Y, Nonaka M, Bito H, Beedle AM, Mori E, Hara Y, De Waard M, Kanagawa M, Itakura M, Takahashi M, Campbell KP & Mori Y (2007). RIM1 confers sustained activity and neurotransmitter vesicle anchoring to presynaptic Ca^{2+} channels. *Nat Neurosci* **10**, 691–701.

Lou X, Scheuss V & Schneggenburger R (2005). Allosteric modulation of the presynaptic Ca^{2+} sensor for vesicle fusion. *Nature* **435**, 497–501.

Meinrenken C, Borst JGG & Sakmann B (2002). Calcium secretion coupling at calyx of Held governed by nonuniform channel-vesicle topography. *J Neurosci* **22**, 1648–1667.

Müller M, Felmy F & Schneggenburger R (2008). A limited contribution of Ca^{2+}-current facilitation to paired-pulse facilitation of transmitter release at the rat calyx of Held. *J Physiol* **586**, 5503–5520.

Naraghi M, Müller TH & Neher E (1998). Two-dimensional determination of the cellular Ca^{2+} binding in bovine chromaffin cells. *Biophys J* **75**, 1635–1647.

Neher E (1998). Usefulness and limitations of linear approximations to the understanding of Ca^{++} signals. *Cell Calcium* **24**, 345–357.

Neher E & Sakaba T (2001). Combining deconvolution and noise analysis for the estimation of transmitter release rates at the calyx of Held. *J Neurosci* **21**, 444–461.

Price GD & Trussell LO (2007). Good players left on the sidelines: why some synaptic vesicles don't get in the game. *Neuron* **53**, 471–473.

Rettig J, Sheng ZH, Kim DK, Hodson CD, Snutch TP & Catterall WA (1996). Isoform-specific interaction of the α_{1A} subunits of brain Ca^{2+} channels with the presynaptic proteins syntaxin and SNAP-25. *Proc Natl Acad Sci U S A* **93**, 7363–7368.

Rodriguez-Contreras A, van Hoeve JS, Habets RL, Locher H & Borst JG (2008). Dynamic development of the calyx of Held synapse. *Proc Natl Acad Sci U S A* **105**, 5603–5608.

Sakaba T (2006). Roles of the fast-releasing and the slowly releasing vesicles in synaptic transmission at the calyx of Held. *J Neurosci* **26**, 5863–5871.

Sakaba T & Neher E (2001). Quantitative relationship between transmitter release and calcium current at the calyx of Held synapse. *J Neurosci* **21**, 462–476.

Schneggenburger R & Neher E (2000). Intracellular calcium dependence of transmitter release rates at a fast central synapse. *Nature* **406**, 889–893.

Schneggenburger R & Neher E (2005). Presynaptic calcium and control of vesicle fusion. *Curr Opin Neurobiol* **15**, 266–274.

Schwarz G (1978). Estimating the dimension of a model. *Ann Statist* **6**, 461–464.

Sheng ZH, Rettig J, Takahashi M & Catterall WA (1994). Identification of a syntaxin-binding site on N-type calcium channels. *Neuron* **13**, 1303–1313.

Steinert JR, Kopp-Scheinpflug C, Baker C, Challiss RA, Mistry R, Haustein MD, Griffin SJ, Tong H, Graham BP & Forsythe ID (2008). Nitric oxide is a volume transmitter regulating postsynaptic excitability at a glutamatergic synapse. *Neuron* **60**, 642–656.

Sun J, Pang ZP, Qin D, Fahim AT, Adachi R & Sudhof TC (2007). A dual-Ca^{2+}-sensor model for neurotransmitter release in a central synapse. *Nature* **450**, 676–682.

Taschenberger H, Leao RM, Rowland KC, Spirou GA & von Gersdorff H (2002). Optimizing synaptic architecture and efficiency for high-frequency transmission. *Neuron* **36**, 1127–1143.

Taschenberger H, Scheuss V & Neher E (2005). Release kinetics, quantal parameters and their modulation during short-term depression at a developing synapse in the rat CNS. *J Physiol* **568**, 513–537.

Taschenberger H & von Gersdorff H (2000). Fine-tuning an auditory synapse for speed and fidelity: developmental changes in presynaptic waveform, EPSC kinetics, and synaptic plasticity. *J Neurosci* **20**, 9162–9173.

Trussell LO (1999). Synaptic mechanisms for coding timing in auditory neurons. *Annu Rev Physiol* **61**, 477–496.

Voets T (2000). Dissection of three Ca^{2+}-dependent steps leading to secretion in chromaffin cells from mouse adrenal slices. *Neuron* **28**, 537–545.

von Gersdorff H, Schneggenburger R, Weis S & Neher E (1997). Presynaptic depression at a calyx synapse: The small contribution of metabotropic glutamate receptors. *J Neurosci* **17**, 8137–8146.

Wadel C, Neher E & Sakaba T (2007). The coupling between synaptic vesicles and Ca^{2+} channels determines fast neurotransmitter release. *Neuron* **53**, 563–575.

Wang L-Y, Neher E & Taschenberger H (2008). Synaptic vesicles in mature calyx of Held synapses sense higher nanodomain calcium concentrations during action potential-evoked glutamate release. *J Neurosci* **28**, 14450–14458.

Wölfel M, Lou X & Schneggenburger R (2007). A mechanism intrinsic to the vesicle fusion machinery determines fast and slow transmitter release at a large CNS synapse. *J Neurosci* **27**, 3198–3210.

Wu LG, Westenbroek RE, Borst JGG, Catterall WA & Sakmann B (1999). Calcium channel types with distinct presynaptic localization couple differentially to transmitter release in single calyx-type synapses. *J Neurosci* **19**, 726–736.

Yang YM & Wang LY (2006). Amplitude and kinetics of action potential-evoked Ca^{2+} current and its efficacy in triggering transmitter release at the developing calyx of Held synapse. *J Neurosci* **26**, 5698–5708.

Yoshikami D, Bagabaldo Z & Olivera BM (1989). The inhibitory effects of omega-conotoxins on Ca channels and synapses. *Ann N Y Acad Sci* **560**, 230–248.

Author contributions

O.K., Y.H. and R.S. designed the research; O.K. and Y.H. performed the experiments and analysed the data; O.K., Y.H. and R.S. contributed to manuscript drafts; R.S. wrote the paper. All the experiments were done at EPFL, Lausanne, Switzerland.

Acknowledgements

We thank Martin Müller for helpful discussions and for providing part of the data shown in Supplemental Fig. 3, and Holger Taschenberger for providing the mEPSC analysis routine. This work was supported by the Swiss National Science Foundation (3100A0-114069), by the Synapsis Foundation, and by the European Commission Coordination Action ENINET (contract number LSHM-CT-2005-19063).